



High Performance and Flexible Electrodeposited Silver Mesh Transparent Conducting Electrodes Based on a Self-Cracking Template

Seoin Kang¹ · Vinaya Kumar Arepalli² · Eunyeong Yang¹ · Sangyeob Lee² · Jung-Sub Wi² · Jae Ho Yun³ · Soomin Song⁴ · Kihwan Kim^{4,5} · Young-Joo Eo^{4,5} · Jun-Sik Cho^{4,5} · Jihye Gwak^{4,5} · Choong-Heui Chung^{1,2}

Received: 6 June 2022 / Accepted: 12 June 2022 / Published online: 11 August 2022
© The Author(s) under exclusive licence to The Korean Institute of Metals and Materials 2022

Abstract

Metal network based transparent conducting electrodes are essential for the future optoelectronic devices due to their mechanical flexibility and compatible with large-scale manufacturing. In this report, we investigated the morphological, optical, electrical, and flexible properties of an electrodeposited silver (Ag) mesh transparent conducting electrodes based on a self-cracking template. An overly coated Ag mesh (ED-TE Ag mesh) was prepared onto glass and PET substrates by the sequential deposition steps including thermal evaporation and electroplating methods. The self-cracking template was lift-off prior to the over coating of Ag by the electrodeposition step. The surface morphologies of ED-TE Ag meshes are smooth and well interconnected. The Ag mesh thickness and line width are typically increased with the electroplating time from 0 s to 30 s. The ED-TE Ag mesh shows higher optoelectronic performance with a larger figure of merit ($2827 (\Omega/\text{sq})^{-1}$) than the individual evaporated Ag mesh ($756 (\Omega/\text{sq})^{-1}$) and the ITO film ($311 (\Omega/\text{sq})^{-1}$). Moreover, the low sheet resistance ($1.01 \Omega/\text{sq}$) of the ED-TE Ag mesh is observed at 30 s. The ED-TE Ag mesh exhibits almost stable resistance to both concave and convex bending tests, even at a smaller radius of curvature ($<2 \text{ mm}$). Thus, these electrodes are more suitable for many flexible device applications like solar cells, displays, etc.

✉ Jihye Gwak
bleucoeur@kier.re.kr

✉ Choong-Heui Chung
choong@hanbat.ac.kr

¹ Department of Materials and Manufacturing Engineering, Hanbat National University, Daejeon 34158, Republic of Korea

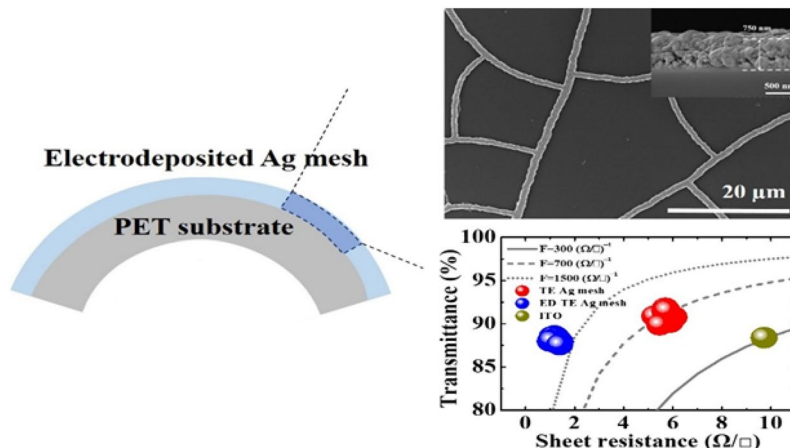
² Department of Materials Science and Engineering, Hanbat National University, Daejeon 34158, Republic of Korea

³ Department of Energy Engineering, Korea Institute of Energy Technology, Naju, Jeonnam 58330, Republic of Korea

⁴ Photovoltaics Research Department, Korea Institute of Energy Research (KIER), Daejeon 34129, Republic of Korea

⁵ Renewable Energy Engineering, University of Science and Technology (UST), Daejeon 34113, Republic of Korea

Graphical abstract



Keywords Transparent conducting electrodes · Crack template · Silver mesh · Electrodeposition · Mechanical flexibility

1 Introduction

Transparent conducting electrodes (TCEs) are important components of optoelectronic devices [1], such as displays [2], touch screens [3], and solar cells [4–6]. Oxide-based materials [7], such as indium tin oxide (ITO) [8], Al-doped zinc oxide (AZO) [9, 10], and F-doped tin oxide (FTO) [11], have been widely used as transparent conductive electrodes (TCEs) because of their high optical transmittance ($\geq 90\%$) in the visible wavelength regime and a low sheet resistance of $10 \Omega \cdot \text{sq}^{-1}$ [12]. However, in the application of flexible and wearable optoelectronic devices [13, 14], these materials cannot be suitable due to their brittleness, and also, large scale bending causes high resistance. Recently, alternative flexible TCEs such as carbon nanotubes (CNTs) [12, 15, 16], graphene [17, 18], conductive polymer materials [19, 20], and metal networks [21–23] have been explored. Among them, metallic networks like metal nanowires and metal mesh can reduce the constraint between transmittance and sheet resistance to some extent and also, because of the hollow metal structures, even they broaden the optical transmission spectrum [1, 24, 25]. Particularly, the Ag metal networks such as nanowires and meshes are widely emerged as the most promising materials in terms of its high electrical conductivity, large area deposition, and superior mechanical flexibility [26–39], and they can successfully replace ITO thin films for thin-film solar cells [30, 31]. Though the Ag nanowires are simple solution processing, they exhibit intrinsic drawbacks of percolation and higher contact resistances between wires [32].

In contrast, the Ag metal mesh can perfectly eliminate the above drawbacks associated with the Ag nanowires.

Moreover, the conductivity of the Ag mesh can be tuned by varying its thickness with no effect on transmittance [28, 33, 34]. The Ag mesh can be prepared by using sacrificial templates such as lithographic patterns, electrospun fiber meshes, and self-cracking networks. Though the lithographic process creates highly controllable periodic patterns, its production is expensive [28]. The self-cracking material based on TiO_2 [14], CA600 [14], albumin, or acrylic resins produces random cracks with a well-uniformly connected network. Physical vapor deposition methods, including thermal evaporation and sputtering, are most widely used to deposit Ag on the self-cracking template [35]. However, the maximum Ag mesh thickness is strongly dependent on the crack width, height, pitch, etc. On the other hand, a direct wet chemical process cannot be used to deposit Ag into the crack networks. Because, the crack templates can be easily peeled off from the supporting substrate in the solution [36]. A higher thickness is necessary to improve the electrical conductivity as well as the optoelectronic performance of the Ag network.

In the present study, an overly coated Ag mesh was prepared by two sequential deposition steps: (1) deposition of Ag on the self-cracking template by thermal evaporation and followed by lift off of the crack template. (2) Ag electrodeposition onto thermally evaporated Ag mesh. The resultant Ag network was denoted as ED-TE Ag mesh. The optical, electrical, and flexible properties of the deposited Ag mesh have been investigated. The ED-TE Ag mesh showed a higher optoelectronic performance than the thermally evaporated Ag mesh (TE Ag mesh) and ITO films. The ED-TE Ag mesh showed excellent flexibility and stable resistance even after bending at a smaller radius of curvature of ~ 2 mm.

2 Experimental Section

2.1 Fabrication of Silver Mesh-Based Transparent Conducting Electrode

A crack template method was used to create the Ag mesh-based network. The process flow of Ag mesh formation using a self-cracking template is shown schematically in Fig. 1. First, a commercially available acrylic based resin (Lubrizol CarboSet CR735) was spin-coated on the glass and PET substrates for 30 seconds at 3000 rpm. After drying at room temperature, the U-shaped grooves completely cracked down to the substrate with a well interconnected crack network spontaneously. This template was coated with silver using a thermal evaporation method. Subsequently, the Ag coated substrate was immersed in acetone and removed the sacrificial template. A thin layer of Ag was deposited on the cracked region, forming a silver mesh. An electrodeposition (ED) was used to enhance the electrical properties of the mesh by increasing the Ag thickness further. In a typical process, a silver solution was prepared by dissolving 7 g of silver cyanide (Acros Organics, 180230500), 15 g of potassium cyanide (Sigma-Aldrich, 207810), 1.5 g of potassium carbonate (Alfa-Aesar, A16625), and 5 g of sodium thiosulfate pentahydrate (Alfa-Aesar, A17914) in 85 ml of DI water. A silver mesh as a working electrode and a silver plate as a reference electrode were then immersed in the silver solution under a constant current source of -4.5 mA.

The total optical transmittance of the deposited Ag mesh was analyzed using a UV–visible spectrometer. The sheet resistance of the Ag mesh was measured using a four-point probe. The morphology of the self-cracking template and the Ag mesh were characterized by using an optical microscope (OM) and field-emission scanning electron microscopy (FE-SEM). The mechanical flexibility was estimated by measuring the surface resistance of ED-TE Ag mesh under both concave and convex bending tests.

3 Results and Discussion

Figure 2 represents the optical microscopic images of the crack template, TE Ag mesh, and ED-TE Ag mesh. Figure 2(a) reveals that the crack-to-crack spacing and crack width of the template are 23.24 μm and 1.85 μm , respectively. From Fig. 2(b) and (c), it is evident that both TE Ag and ED-TE Ag meshes exhibit a uniform distribution of Ag with a well interconnected mesh network throughout the surface. However, the electrodeposited Ag mesh line width seems to become wider than the TE Ag mesh. Figure 3 illustrates the surface and cross-sectional morphologies of the TE and ED-TE Ag meshes grown at 0 s and 30 s. From Fig. 3(a) and (b), it is observed that both meshes seem to have many polygon areas with seamless junctions of the Ag networks. In addition to the smooth surface, the electrodeposition directly expands the Ag mesh line width. As electrodeposition time rises from 0 s to 30 s the Ag mesh line width increases from 0.85 μm to 1.53 μm . As a result, the

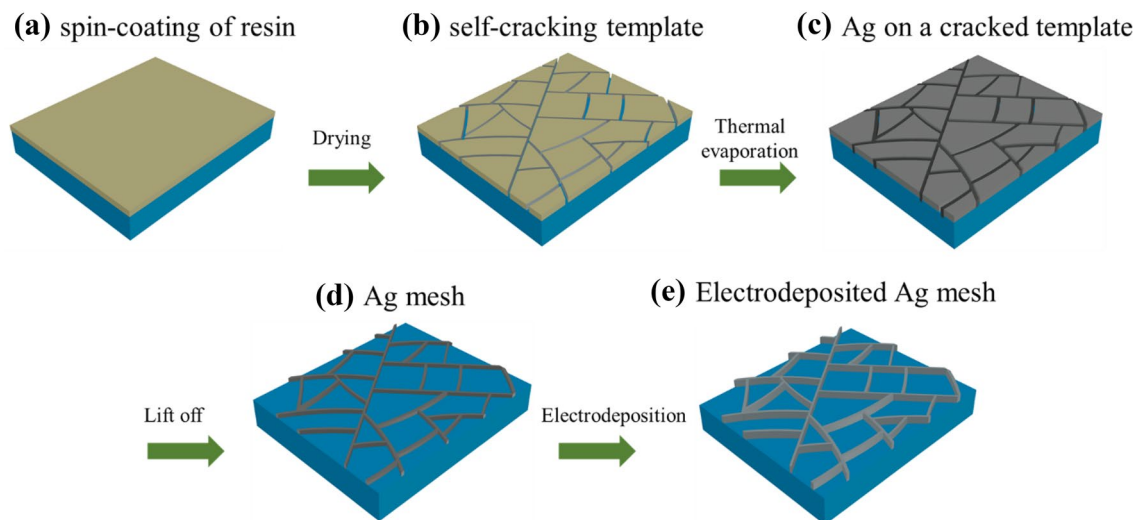


Fig. 1 Schematic illustration of the Ag mesh transparent conducting electrode processing steps. **a** Spin coating of acrylic resin layer on PET substrate, **b** generation of self-cracking template on drying at room temperature, **c** thermal evaporation of Ag metal on the self-

cracked template, **d** Formation of the Ag mesh network after lift-off process, and **e** A thick Ag mesh by electrodeposition of Ag onto the thermally evaporated Ag network

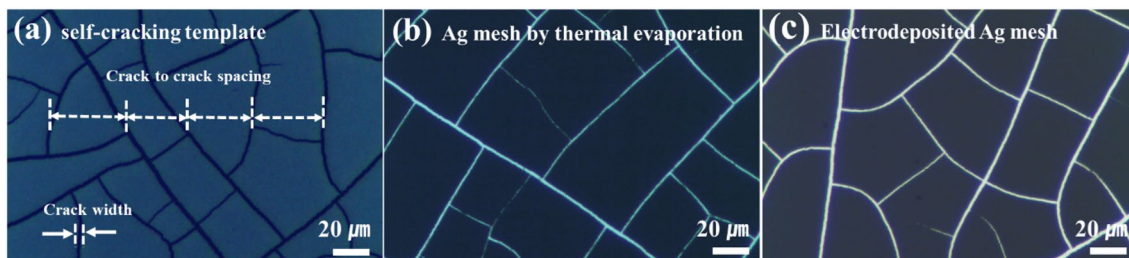
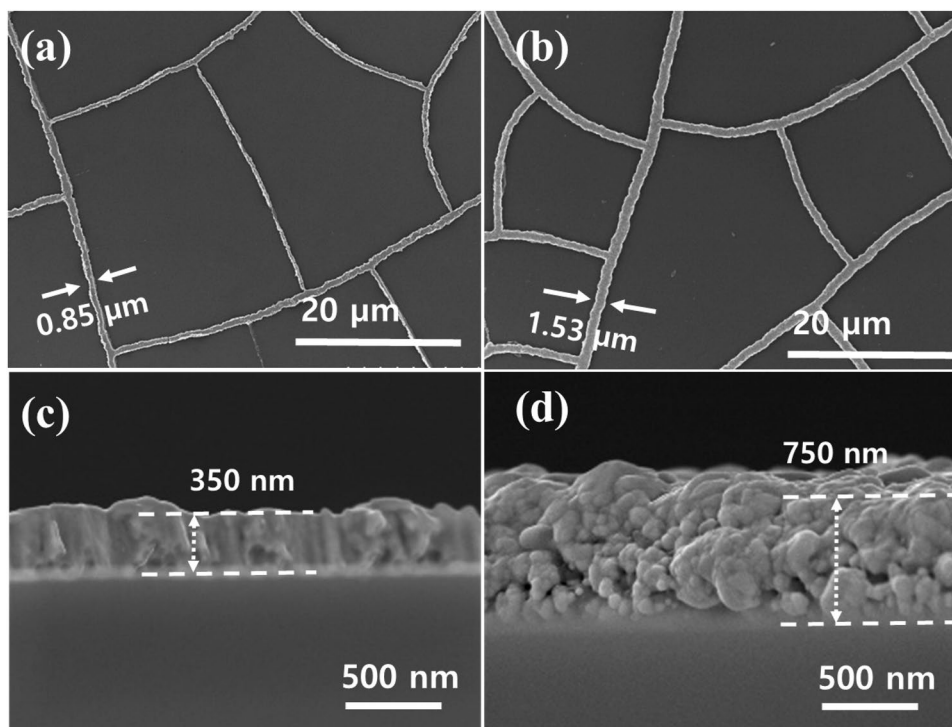


Fig. 2 Optical microscopic images of the **a** crack template, **b** thermally evaporated Ag mesh, and **c** ED-TE Ag mesh

Fig. 3 Surface and cross-sectional SEM images of the electrodeposited Ag mesh grown at (a, c) 0 s and (b, d) 30 s



average spacing between polygons of the Ag mesh is reduced from 22.96 μm to 15.0 μm. Figure 3(c) and 3(d) denotes an increase in the thickness of the Ag mesh from 350 nm to 750 nm grown at 0 s and 30 s, respectively. Besides, the electrodeposited Ag uniformly covers the TE Ag mesh and it becomes a single Ag layer at 30 s growth time.

Figure 4(a) shows the relationship between the Ag thickness and electroplating time. The initial thickness of the Ag at 0 s is 350 nm (TE Ag mesh). The Ag thickness gradually increases to 450 nm, 600 nm, and 750 nm with increasing electroplating time to 10 s, 20 s, and 30 s, respectively. Figure 4(b) indicates the dependence of the sheet resistance of the ED-TE Ag mesh on electroplating time. As the electroplating time varies from 0 s to 10 s, 20 s, and 30 s, the corresponding sheet resistance values of the Ag mesh reduce from 5.7 Ω.sq⁻¹ to 2.48, 1.85, and 1.01 Ω.sq⁻¹, respectively. This result is consistent with the thickness differences of the

Ag meshes. Furthermore, because of the random structure of the Ag mesh network, charge carriers can be smoothly transported through these networks, resulting in a much lower sheet resistance than ITO films (9.72 Ω.sq⁻¹).

Figure 4(c) depicts the variation of transmittance at 550 nm as a function of the electroplating time. As the electroplating time goes from 0 s to 30 s, the transmittance (@550 nm) of the ED-TE Ag mesh slightly drops from 91.8% to 88.9%, 88.7%, and 88%, respectively. When compared to TE Ag, the addition of electrodeposited Ag not only increases the thickness but also expands the mesh line width to some extent (Fig. 3b). As a result, the transmittance loss of the ED-TE Ag mesh increases from 2.9% for 10 s to 3.8% for 30 s. However, at 10 s and 20 s, the Ag meshes exhibit almost the same transmittance as ITO film. The Ag mesh with a larger thickness (750 nm; 30 s) exhibits higher optical transmittance (88%) than the previously reported transmittance (86.3%) of a thin 100 nm thick

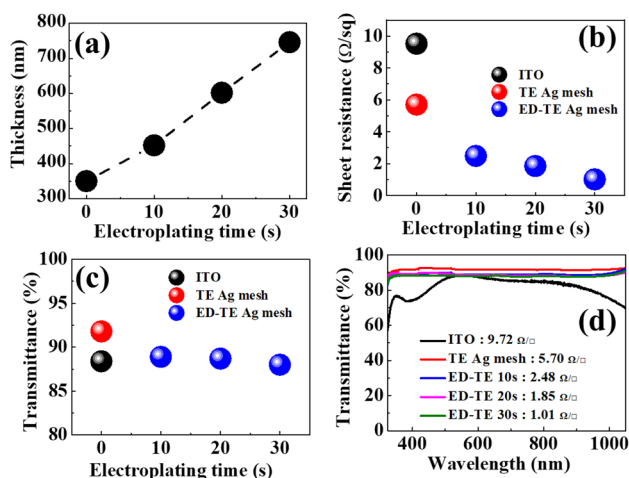


Fig. 4 Plots of **a** electrodeposition time vs. Ag thickness, **b** electrodeposition time vs. sheet resistance, **c** electrodeposition time vs. transmittance at 550 nm wavelength, and the spectra of **d** optical wavelength vs. transmittance of the Ag mesh

sputtered Ag network [36]. On the other hand, the total transmittance of the Ag meshes is shown in Fig. 4(d). Because of the sparse nature of the ED-TE and TE Ag meshes, the average transmittance is almost constant (88.9%) in the wavelength range of 325–1000 nm. Whereas the transmittance of ITO thin film slightly drops at shorter and longer wavelengths.

It is clear that the reduction in sheet resistance is directly proportional to an increase in Ag mesh thickness. Whereas the fall in transmittance is directly proportional to an increase in the Ag mesh line width. Both sheet resistance and transmittance values decrease gradually as the electroplating time goes from 0 s to 30 s. However, more loss is observed in the sheet resistance than in the optical transmittance. To investigate the further improvements in the optoelectronic performance of the ED-TE Ag mesh compared to TE Ag and ITO, we calculated the figure of merit (*FoM*). The *FoM* is defined as the ratio of electrical conductance to optical conductance (σ_{dc}/σ_{opt}) and can be evaluated by using the following expression [30, 31],

$$FoM = \frac{\sigma_{dc}}{\sigma_{opt}} = \frac{188.5}{R_s \cdot (T_{550}^{-1/2} - 1)} \quad (1)$$

where T_{550} is the optical transmittance at a wavelength of 550 nm and R_s is the sheet resistance. The estimated *FoM* is as shown in Fig. 5(a) by plotting the transmittance versus sheet resistance (R_s) for the ED-TE Ag mesh and TE Ag mesh. Figure 5(b) also depicts the electroplating time-dependent *FoM*. Figure 5(a) and (b) clearly evident that the ED-TE Ag mesh outperformed the other transparent electrodes. The *FoMs* of both TE Ag mesh and a reference ITO electrode were ~ 756 and 311 (Ω/sq) $^{-1}$. Whereas the *FoMs* of ED-TE Ag mesh reaches to 1254, 1649, and 2827 (Ω/sq) $^{-1}$ with 10 s, 20 s, and 30 s deposition times, respectively. Based

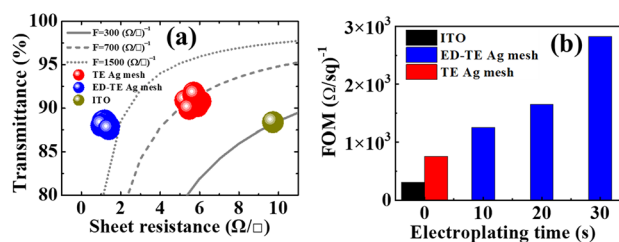


Fig. 5 plots of **a** optical transmittance vs. sheet resistance and **b** electrodeposition time vs. figure of merit of the Ag mesh

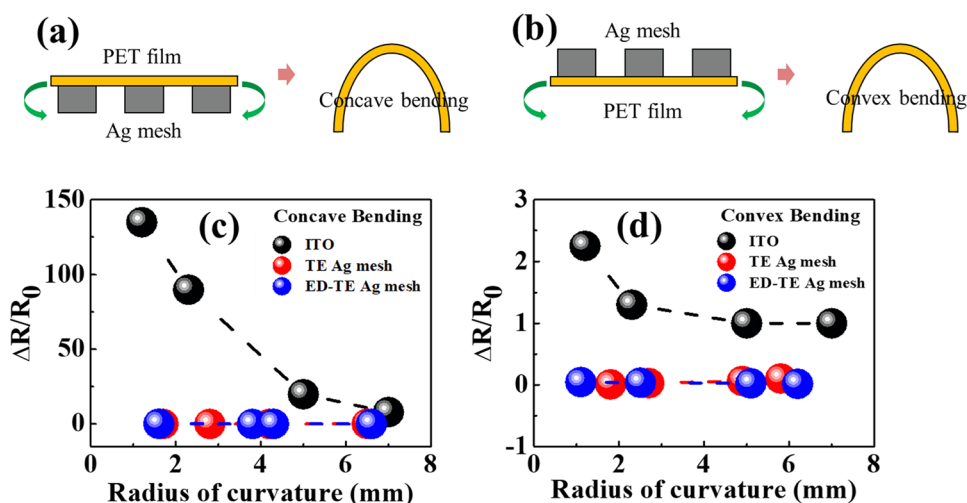
on these *FoM* values, the ED-TE Ag mesh can be used as a highly efficient transparent conducting electrode than the TE Ag mesh and ITO films.

The mechanical flexibility of the ED-TE Ag mesh is compared with that of the TE Ag network and the reference ITO film by performing a bending test. Samples were prepared on the PET substrates. Figure 6(a) and (b) represents the schematic view of concave and convex bending process. Figure 6(c) and (d) show the results of mechanical stability under cyclic concave and convex bending tests. The samples are repeatedly bent at different radius of curvatures from 1 mm to 7 mm. The ED-TE Ag mesh and TE Ag, exhibit almost no noticeable change in resistance, even at a smaller radius of curvature (< 2 mm). While the ITO film shows an increased resistance even at the larger radius of curvature (5 mm). Moreover, the change in resistance is much higher in the concave bending than in the convex bending for the ITO film.

4 Conclusion

We fabricated the Ag mesh onto glass and PET substrates by the sequential deposition steps of thermal evaporation and electroplating techniques. A self-cracking template was used to form a smooth and well interconnected Ag mesh network. However, this template was removed before to the over coating of Ag by electrodeposition. The optical and electrical properties of the ED-TE Ag mesh were studied as a function of electrodeposition time. The ED-TE Ag mesh thickness and line width were increased with an increase in time from 0 s to 30 s. The ED-TE Ag mesh showed a higher figure of merit in terms of optoelectronic performance than the TE Ag mesh and ITO films. The ED-TE Ag mesh deposited at 30 s showed a lower sheet resistance of $1.01 \Omega/\text{sq}$ and 88% of transmittance at 550 nm wavelength. Even at a smaller radius of curvature (< 2 mm), the ED-TE Ag mesh showed almost stable resistance to both concave and convex bending tests. Therefore, this ED-TE Ag mesh is the best choice to use as an

Fig. 6 Comparison of mechanical flexibility; Plots of radius of curvature vs. change in resistance by **a** concave bending and **b** convex bending of the Ag mesh samples



efficient flexible transparent electrode for optoelectronic applications.

Acknowledgments This research was supported by the framework of the Research and Development Program of the Korea Institute of Energy Research (KIER C2-2401-01), the Basic Science Research Program through the National Research Foundation of Korea (NRF) that is funded by the Ministry of Science and ICT (Grant No. NRF-2021R1A2C1005815), and Regional Innovation Strategy (RIS) through the National Research Foundation of Korea (NRF) funded by the Ministry of Education (MOE) (2021RIS-004).

Declarations

Conflict of interests We declare that this manuscript is original and has not been published before and is not currently being considered for publication elsewhere. The authors declare that they have no conflicts of interest to disclose that are relevant to the content of this article.

Ethical approval All authors have participated in (a) conception and design, or analysis and interpretation of the data; (b) drafting the article or revising it critically for important intellectual content; and (c) approval of the final version.

References

1. Hecht, D.S., Hu, L., Irvin, G.: Emerging transparent electrodes based on thin films of carbon nanotubes, graphene, and metallic nanostructures. *Adv. Mater.* **23**, 1482–1513 (2011)
2. Rao, K.D.M., Hunger, C., Gupta, R., Kulkarni, G.U., Thelakkat, M.: A cracked polymer templated metal network as a transparent conducting electrode for ITO-free organic solar cells. *Phys. Chem. Chem. Phys.* **16**, 15107–15110 (2014)
3. Bae, S., Kim, H., Lee, Y., Xu, X., Park, J.S., Zheng, Y., Balakrishnan, J., Lei, T., Kim, H.R., Song, Y.I., Kim, Y.J., Kim, K.S., Ozyilmaz, B., Ahn, J.H., Hong, B.H., Iijima, S.: Roll-to-roll production of 30-inch graphene films for transparent electrodes. *Nat. Nanotechnol.* **5**, 574–578 (2010)
4. Fortunato, E., Barquinha, P., Martins, R.: Oxide semiconductor thin-film transistors: a review of recent advances. *Adv. Mater.* **24**, 2945–2986 (2012)
5. Ellmer, K.: Past achievements and future challenges in the development of optically transparent electrodes. *Nat. Photonics* **6**, 809–817 (2012)
6. Jang, J., Lee, J.S., Hong, K.H., Lee, D.K., Song, S., Kim, K., Eo, Y.J., Yun, J., Chung, C.H.: Cu(In, Ga) S_2 thin film solar cells with solution processed silver nanowire composite window layers: buffer/window junctions and their effects. *Sol. Energy Mater. Sol. Cells* **170**, 60–67 (2017)
7. Kumar, A., Zhou, C.: The race to replace tin-doped indium oxide: which material will win? *ACS Nano* **4**, 11–14 (2010)
8. Yang, L., Zhang, T., Zhou, H., Price, S.C., Wiley, B.J., You, W.: Solution-processed flexible polymer solar cells with silver nanowire electrodes. *ACS Appl. Mater. Interfaces* **3**, 4075–4084 (2011)
9. Chung, C.H.: Lateral photocurrent method for directly measuring the sheet resistance of a junction partner for a chalcogenide light absorber in a thin-film solar cell. *Phys. Rev. Appl.* **17**, 1 (2022)
10. Cho, K.S., Jang, J., Park, J.H., Lee, D.K., Song, S., Kim, K., Eo, Y.J., Yun, J.H., Gwak, J., Chung, C.H.: Optimal CdS buffer thickness to form high-quality CdS/Cu(In, Ga) S_2 junctions in solar cells without plasma damage and shunt paths. *ACS Omega* **5**, 23983–23988 (2020)
11. Way, A., Luke, J., Evans, A.D., Li, Z., Kim, J.S., Durrant, J.R., Hin Lee, H.K., Tsoi, W.C.: Fluorine doped tin oxide as an alternative of indium tin oxide for bottom electrode of semi-transparent organic photovoltaic devices. *AIP Adv.* **9**(8), 085220 (2019)
12. Geng, H.Z., Kim, K.K., So, K.P., Lee, Y.S., Chang, Y., Lee, Y.H.: Effect of acid treatment on carbon nanotube-based flexible transparent conducting films. *J. Am. Chem. Soc.* **129**, 7758–7759 (2007)
13. Tenent, R.C., Barnes, T.M., Bergeson, J.D., Ferguson, A.J., To, B., Gedvilas, L.M., Heben, M.J., Blackburn, J.L.: Ultrasmooth, large-area, high-uniformity, conductive transparent single-walled-carbon-nanotube films for photovoltaics produced by ultrasonic spraying. *Adv. Mater.* **21**, 3210–3216 (2009)
14. Han, B., Pei, K., Huang, Y., Zhang, X., Rong, Q., Lin, Q., Guo, Y., Sun, T., Guo, C., Carnahan, D., Giersig, M., Wang, Y., Gao, J., Ren, Z., Kempa, K.: Uniform self-forming metallic network as a high-performance transparent conductive electrode. *Adv. Mater.* **26**, 873–877 (2014)
15. Tenent, R.C., Barnes, T.M., Bergeson, J.D., Ferguson, A.J., To, B., Gedvilas, L.M., Heben, M.J., Blackburn, J.L.: Ultrasmooth,

- large-area, high-uniformity, conductive transparent single-walled-carbon-nanotube films for photovoltaics produced by ultrasonic spraying. *Adv. Mater.* **21**, 3210–3216 (2009)
16. Kim, J., Yun, A.J., Park, B., Kim, J.: Recent progress in carbon electrodes for efficient and cost-benign perovskite optoelectronics. *Electron. Mater. Lett.* **18**, 232–255 (2022)
 17. Kim, K.S., Zhao, Y., Jang, H., Lee, S.Y., Kim, J.M., Kim, K.S., Ahn, J.H., Kim, P., Choi, J.Y., Hong, B.H.: Large-scale pattern growth of graphene films for stretchable transparent electrodes. *Nature* **457**, 706–710 (2009)
 18. Yu, H.K.: Copper micro-labyrinth with graphene skin: new transparent flexible electrodes with ultimate low sheet resistivity and superior stability. *Nanomaterials* **6**, 161 (2016)
 19. Kim, N., Kee, S., Lee, S.H., Lee, B.H., Kahng, Y.H., Jo, Y.R., Kim, B.J., Lee, K.: Highly conductive PEDOT:PSS nanofibrils induced by solution-processed crystallization. *Adv. Mater.* **26**, 2268–2272 (2014)
 20. Mengistie, D.A., Ibrahim, M.A., Wang, P.C., Chu, C.W.: Highly conductive PEDOT:PSS treated with formic acid for ITO-free polymer solar cells. *ACS Appl. Mater. Interfaces* **6**, 2292–2299 (2014)
 21. Cheong, H.G., Song, D.W., Park, J.W.: Transparent film heaters with highly enhanced thermal efficiency using silver nanowires and metal/metal-oxide blankets. *Microelectron. Eng.* **146**, 11–18 (2015)
 22. Hsu, P.C., Kong, D., Wang, S., Wang, H., Welch, A.J., Wu, H., Cui, Y.: Electrolessly deposited electrospun metal nanowire transparent electrodes. *J. Am. Chem. Soc.* **136**, 10593–10596 (2014)
 23. Chee, S.S., Kim, H., Son, M., Ham, M.H.: Aspect ratio control of copper nanowire via solution process and its flexible transparent conductive electrode applications. *Electron. Mater. Lett.* **16**, 404–410 (2020)
 24. Hu, M., Gao, J., Dong, Y., Li, K., Shan, G., Yang, S., Li, R.K.Y.: Flexible transparent PES/silver nanowires/PET sandwich-structured film for high-efficiency electromagnetic interference shielding. *Langmuir* **28**, 7101–7106 (2012)
 25. Jung, E.D., Nam, Y.S., Seo, H., Lee, B.R., Yu, J.C., Lee, S.Y., Kim, J.Y., Park, J.U., Song, M.H.: Highly efficient flexible optoelectronic devices using metal nanowire-conducting polymer composite transparent electrode. *Electron. Mater. Lett.* **11**, 906–914 (2015)
 26. Yang, C., Merlo, J.M., Kong, J., Xian, Z., Han, B., Zhou, G., Gao, J., Burns, M.J., Kempa, K., Naughton, M.J.: All-solution-processed, scalable, self-cracking ag network transparent conductor. *Phys. Status Solidi A* **215**, 1–6 (2018)
 27. Lee, S., Lee, J.S., Jang, J., Hong, K.H., Lee, D.K., Song, S., Kim, K., Eo, Y.J., Yun, J.H., Gwak, J., Chung, C.H.: Robust nanoscale contact of silver nanowire electrodes to semiconductors to achieve high performance chalcogenide thin film solar cells. *Nano Energy* **53**, 675–682 (2018)
 28. Yang, M.K., Lee, J.K.: CNT/AgNW multilayer electrodes on flexible organic solar cells. *Electron. Mater. Lett.* **16**, 573–578 (2020)
 29. Prabukumar, C., Bhat, K.U.: Beneficial effect of manganese(ii) ions on the morphology of polyol synthesised silver nanowires. *Electron. Mater. Lett.* **16**, 264–275 (2020)
 30. Lee, S., Jang, J., Park, T., Park, Y.M., Park, J.S., Kim, Y.K., Lee, H.K., Jeon, E.C., Lee, D.K., Ahn, B., Chung, C.H.: Electrodeposited silver nanowire transparent conducting electrodes for thin-film solar cells. *ACS Appl. Mater. Interfaces* **12**, 6169–6175 (2020)
 31. Cho, K.S., Kang, S., Oh, Y.J., Park, J.S., Lee, S., Wi, J.S., Park, J.H., Song, S., Kim, K., Eo, Y.J., Yun, J.H., Gwak, J., Cho, J.S., Chung, C.H.: Hierarchical silver network transparent conducting electrodes for thin-film solar cells. *ACS Appl. Electron. Mater.* **4**, 823–830 (2022)
 32. Han, Y., Lin, J., Liu, Y., Fu, H., Ma, Y., Jin, P., Tan, J.: Crackle template based metallic mesh with highly homogeneous light transmission for high-performance transparent EMI shielding. *Sci. Rep.* **6**, 1–11 (2016)
 33. Rao, K.D.M., Gupta, R., Kulkarni, G.U.: Fabrication of large area, high-performance, transparent conducting electrodes using a spontaneously formed crackle network as template. *Adv. Mater. Interfaces* **1**, 1–7 (2014)
 34. Kiruthika, S., Rao, K.D.M., Kumar, A., Gupta, R., Kulkarni, G.U.: Metal wire network based transparent conducting electrodes fabricated using interconnected crackled layer as template. *Mater. Res. Express* **1**, 026301 (2014)
 35. Xian, Z., Han, B., Li, S., Yang, C., Wu, S., Lu, X., Gao, X., Zeng, M., Wang, Q., Bai, P., Naughton, M.J., Zhou, G., Liu, J.M., Kempa, K., Gao, J.: A practical ITO replacement strategy: sputtering-free processing of a metallic nanonetwork. *Adv. Mater. Technol.* **2**, 1–6 (2017)
 36. Cui, M., Zhang, X., Rong, Q., Nian, L., Shui, L., Zhou, G., Li, N.: High conductivity and transparency metal network fabricated by acrylic colloidal self-cracking template for flexible thermochromic device. *Org. Electron.* **83**, 1–6 (2020)

Publisher's Note Springer Nature remains neutral with regard to jurisdictional claims in published maps and institutional affiliations.

Springer Nature or its licensor holds exclusive rights to this article under a publishing agreement with the author(s) or other rightsholder(s); author self-archiving of the accepted manuscript version of this article is solely governed by the terms of such publishing agreement and applicable law.